HAL
open science

Precision measurements of electric-field-induced frequency displacements of an ultranarrow optical transition in ions in a solid

S. Zhang, N. Lučić, N. Galland, R. Le Targat, P. Goldner, B. Fang, S. Seidelin, Y. Le Coq

To cite this version:

S. Zhang, N. Lučić, N. Galland, R. Le Targat, P. Goldner, et al.. Precision measurements of electric-field-induced frequency displacements of an ultranarrow optical transition in ions in a solid. Applied Physics Letters, 2020, 117 (22), pp.221102. 10.1063/5.0025356 . hal-03065368

HAL Id: hal-03065368

https://hal.science/hal-03065368v1

Submitted on 11 Aug 2023

HAL is a multi-disciplinary open access archive for the deposit and dissemination of scientific research documents, whether they are published or not. The documents may come from teaching and research institutions in France or abroad, or from public or private research centers.

L'archive ouverte pluridisciplinaire **HAL**, est destinée au dépôt et à la diffusion de documents scientifiques de niveau recherche, publiés ou non, émanant des établissements d'enseignement et de recherche français ou étrangers, des laboratoires publics ou privés.

Applied Physics Letters ARTICLE scitation.org/journal/apl

Precision measurements of electric-field-induced frequency displacements of an ultranarrow optical transition in ions in a solid

Cite as: Appl. Phys. Lett. **117**, 221102 (2020); doi: 10.1063/5.0025356
Submitted: 14 August 2020 · Accepted: 13 November 2020 ·
Published Online: 30 November 2020

View Online Export Citation CrossMark

S. Zhang,[1] N. Lučić,[1] N. Galland,[1,2] R. Le Targat,[1] P. Goldner,[3] B. Fang,[1] S. Seidelin,[2,a)] and Y. Le Coq[1]

AFFILIATIONS

[1]LNE-SYRTE, Observatoire de Paris, Université PSL, CNRS, Sorbonne Université, 75014 Paris, France
[2]Univ. Grenoble Alpes, CNRS, Grenoble INP and Institut Néel, 38000 Grenoble, France
[3]Chimie ParisTech, Université PSL, CNRS, Institut de Recherche de Chimie Paris, 75005 Paris, France

[a)]Author to whom correspondence should be addressed: signe.seidelin@neel.cnrs.fr

ABSTRACT

We report a series of measurements of the effect of an electric field on the frequency of the ultranarrow linewidth $^7F_0 \rightarrow {}^5D_0$ optical transition of Eu^{3+} ions in an Y_2SiO_5 matrix at cryogenic temperatures. We provide linear Stark coefficients along two dielectric axes and for the two different substitution sites of the Eu^{3+} ions, with an unprecedented accuracy and an upper limit for the quadratic Stark shift. The measurements, which indicate that the electric field sensitivity is a factor of seven larger for site 1 relative to site 2 for a particular direction of the electric field, are of direct interest in the context of both quantum information processing and laser frequency stabilization with rare-earth doped crystals, in which electric fields can be used to engineer experimental protocols by tuning transition frequencies.

Published under license by AIP Publishing. https://doi.org/10.1063/5.0025356

11 August 2023 11:59:53

Optically addressable ions as dopants in solids provide an interesting framework for a wide range of contemporary applications in physics. In particular, rare-earth ions in a crystalline matrix are popular candidates for a steadily growing number of applications due to their outstanding coherence properties.[1–5] Applications include both classical[6,7] and quantum[8–12] information processing schemes, quantum optical memories,[13–15] and laser stabilization techniques.[16–18]

In this work, we use the 580 nm optical $^7F_0 \rightarrow {}^5D_0$ transition in Eu^{3+} ions in an Y_2SiO_5 host matrix (Eu:YSO). This transition has an ultranarrow linewidth, potentially down to 122 Hz at 1.4 K with a magnetic field of 100 G.[2] The Eu^{3+} ions can substitute for Y^{3+} ions in two different crystallographic sites, referred to as sites 1 and 2, with vacuum wavelengths of 580.04 nm and 580.21 nm, respectively, and we here investigate both sites. We have recently demonstrated that the optical transition frequency of the ions can be modulated by applying mechanical stress on the crystalline matrix,[19,20] which makes the system promising for optomechanics experiments in which a mechanical motion couples to the ion frequency.[21,22] An alternative way of controlling the frequency is based on the Stark effect, in which an external electric field interacts with the electric dipole moment involved in the transition.[23,24] In the Eu:YSO system, the Stark coefficients for the optical transition have so far been measured with a limited precision and only in one of the two different substitution sites.[25,26] Here, the technique of spectral hole burning (see later), combined with the use of an ultranarrow linewidth laser, allows us to not only obtain more accurate values for the already measured site but also provide measurements for the other much less sensitive site, which, thus, requires a higher precision in order to assess the corresponding Stark coefficient.

To study the influence of the electrical field (E-field), we use the technique of spectral hole burning, which allows us to work with a large ensemble of ions without being limited by the inhomogeneous broadening of the collective absorption line, which is of the order of 2 GHz in our case for 0.1-at.% europium doping. More precisely, the $^7F_0$ ground state consists of 3 hyperfine states [Fig. 1(a)], with mutual separations in the range of 30–100 MHz..[1] Spectral holes are formed by pumping the ions resonantly from the $^7F_0$ to $^5D_0$ state, from where they decay radiatively, mainly to the $^7F_1$ state[27] before decaying non-radiatively to the three hyperfine states in the $^7F_0$ manifold. Optical pumping prevents population build-up at the hyperfine level with which the pump beam is resonant, creating a transparent window in the inhomogeneous profile at this exact frequency. By subsequently scanning the probe laser in the neighborhood of the pump-laser frequency, the shape and frequency of the spectral hole can be recorded. A spectral hole represents approximately 10^{13} Eu^{3+} ions.

Published under license by AIP Publishing

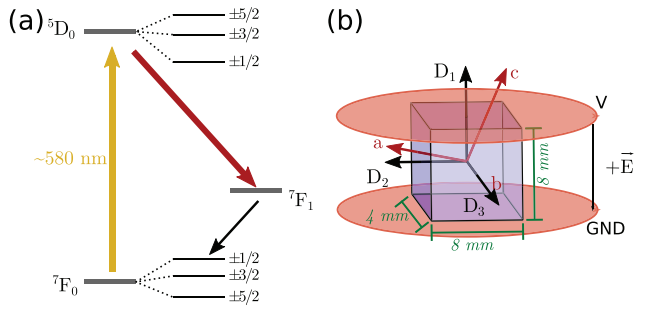

FIG. 1. Ion level structure and crystal axes. In (a), the energy diagram of the Eu^{3+} ions is shown. After resonantly pumping at 580 nm, the ions decay radiatively primarily to $^7F_1$ and then non-radiatively to one of the hyperfine states that are not resonant with the pump beam, leaving behind a sharp hole in the absorption profile. In (b), we show the Y_2SiO_5 crystal, which is cut parallel to the 3 dielectric axes, D_1, D_2, and D_3 (which is parallel to the crystalline *b*-axis and the *a* and *c* axes lying in the D_1, D_2 plane), as well as the electrodes allowing the application of an electric field *E* (here, shown parallel to the D_1) axis due to an electric potential *V*.

Our experimental setup has recently been described in detail elsewhere[18,19,28] and will be only briefly summarized in the following. We use two diode lasers (referred to as master and slave) at 1160 nm. The master laser is frequency locked to an ultra-stable Fabry–Pérot reference optical cavity by the Pound–Drever–Hall technique, allowing for a frequency instability below 10^{-14} for time scales of 1–100 s and a few Hz laser linewidths. The slave laser is phase locked to the master laser with a tunable frequency offset. The slave laser possesses the same stability as the master, but its frequency is continuously tunable in a range of several GHz. Both of them are subsequently frequency doubled to reach 580 nm, with an output intensity of approximately 5 mW. Moreover, an acousto-optic modulator allows us to scan the slave-laser frequency across the spectral structures with a range of approximately 1 MHz. A high stability (in fact, absolute) optical frequency measurement is provided when necessary by comparing the slave laser against a primary frequency reference via an optical frequency comb. Avalanche photodiodes are used to measure the intensity of the slave laser before and after passing through the crystal, thereby deducing the shape and position of the spectral hole. For maximum absorption[27] (for both burning and probing), we propagate the laser beam parallel to the crystallographic *b*-axis and maintain the laser polarization parallel to the dielectric D_1 axis [Fig. 1(b)]. In this work, the pump and the probe beams are collimated and diaphragmed by an iris of 2 mm diameter (a fourth of the crystal width and height) and kept in the center of the crystal in order to minimize surface effects. The crystal is maintained at 3.2 K in a closed-loop cryostat resting on an active vibration isolation platform. Under these conditions, we obtain spectral holes with a full width at half maximum (FWHM) of about 3–5 kHz.

To apply a homogeneous E-field, we use two circular electrodes (31 mm in diameter) above and below the crystal as shown in Fig. 1(b). As the electric permittivity of the crystal is a factor of ten larger than that of vacuum, it is crucial to avoid gaps between electrodes and the crystal. We use a thin (<0.1 mm) layer of silver lacquer to bring the crystal into direct contact with the electrodes. The distance between the electrodes is consequently the same as the height of the crystal (with the electrodes being extended to the surface of the crystal due to the silver lacquer), which is equal to about 8 mm. To study the linear Stark regime, we burn a spectral hole in the absence of an E-field, then apply a voltage ranging from 0 to 28 V, giving rise to an electric field in the range of 0–3500 V m^{-1}, and observe the influence on the spectral hole.

The YSO crystal is monoclinic and exhibits a C_{2h} symmetry. Both the nonequivalent crystallographic sites of the Eu^{3+} ions are of C_1 symmetry. In the general case of an application of an E-field with an arbitrary direction, the crystal symmetry gives rise to four possible nonequivalent orientations of the electric dipole moment difference between the ground and excited states ($\delta\vec{\mu}_i$, i = 1, 2, 3, 4) for each site, arising from the order of the crystal symmetry group (4) divided by the order of the symmetry group of the crystal site (1), see Fig. 2(a). Thus, in the general case, the presence of an arbitrary electric field will split a spectral hole into four components.[30] Because of the centrosymmetric crystal space group, the splitting of the spectral hole will to first order remain symmetric in frequency around zero.

We will determine the Stark effect for an E-field parallel to either the D_1 or D_2 axis and, thus, in both cases, perpendicular to the crystal *b*-axis that coincides with the C_2 rotational symmetry axis. As the mirror symmetry plane of the crystal is perpendicular to the C_2 rotation axis, the E-field is, thus, contained within this plane in our case, as illustrated in Fig. 2(b). This means that the component of a given electric dipole moment perpendicular to the mirror plane is not influenced by our E-field, and thus, the splitting arising from the mirror symmetry vanishes. Therefore, in all our measurements, the spectral hole only splits into two components, arising from the C_2 rotation symmetry alone.

This twofold splitting into a positive and a negative frequency branch is illustrated for an electric field applied along the D_1 direction in Fig. 3. Here, the transmittance *T* of the crystal is plotted as a function of frequency difference *f* with respect to the hole burning frequency, i.e., $f_0 \equiv 0$, where the initial spectral hole burning occurred, for 6 different values of the applied E-field for the two different crystal sites. The center frequency of each peak is then obtained by a double Lorentzian fit of the transmittance, $T(f) = A + B/(1 + 4(f - f_+)^2/\gamma^2) + C/(1 + 4(f - f_-)^2/\gamma^2)$, where f_+ and f_- denote the center frequency of the two branches, γ is the (common) FWHM of the two Lorentzian, and *A*, *B*, and *C* take into account the offset and normalization of *T*(*f*).

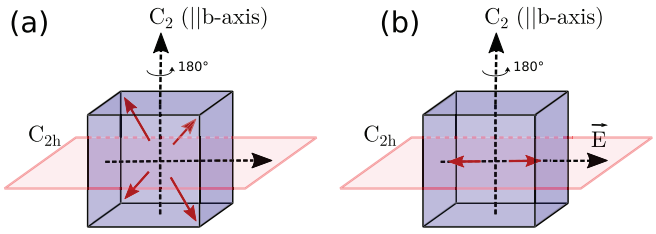

FIG. 2. The symmetry operations of the YSO crystal. In (a), we show the general case, where each $\delta\vec{\mu}_i$ is related by symmetry operations to 4 nonequivalent dipoles. In part (b), we show that when considering the projection of the dipole moment on an axis perpendicular to the C_2 rotation axis (thus contained within the horizontal symmetry plane), this number is reduced to 2. Note that the crystal has been rotated by 90° relative to Fig. 1 in order to follow the usual convention for which the C_2 rotation axis is vertical.

11 August 2023 11:59:53

Published under license by AIP Publishing

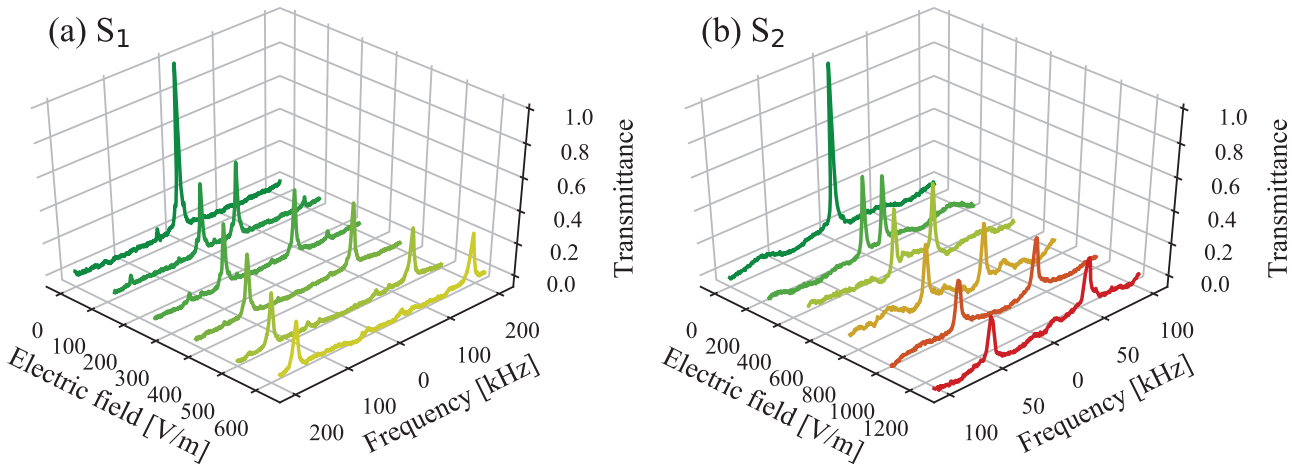

FIG. 3. Transmittance of an Eu^{3+}-doped crystal containing a spectral hole as a function of the electric field applied along the D_1-axis for site 1 (a) and site 2 (b). At zero field, the spectral hole exhibits a linewidth below 5 kHz. When an E-field is applied, the spectral structure splits into two components, of which the difference in frequency increases as the E-field is gradually incremented.

These frequency shifts are then plotted as a function of the E-field in Fig. 4, for an E-field aligned along either the D_1 or D_2 direction and in each case for both crystal sites. Each point in this figure is the average of two separate measurement sequences or more (a data acquisition sequence lasts for approximately 30 min). For each sequence, the shift for each data point is half the frequency difference between the positive and negative branch peak centers, i.e., $\delta f_1 = (f_+ - f_-)/2$ (thereby ensuring a negligible effect of slow frequency drifts of the reference Fabry–Pérot cavity, as such a drift would shift both peaks by the same amount in the same direction). The error bars, which are shown on the data and are used in the fit algorithm, are estimated individually for each curve, as the noise floor (data baseline) varies from scan to scan and adds to the uncertainty on the determination of the central frequency. They correspond to approximately one tenths of the FWHM of the spectral structures in Fig. 3. In order to obtain the linear Stark coefficients, we initially assume that the effect is purely linear and fit the data accordingly with a purely linear model $\delta f_1 = A_1 E$ using a least squares method. The linear Stark coefficients A_1 are given in Table I. Our measurement of the coefficient for site 1 corresponding to an E-field parallel to the D_1-axis is consistent with the earlier, less accurate measurement reported in Ref. 26 (0.27 kHz m V^{-1} with no explicit error bar).

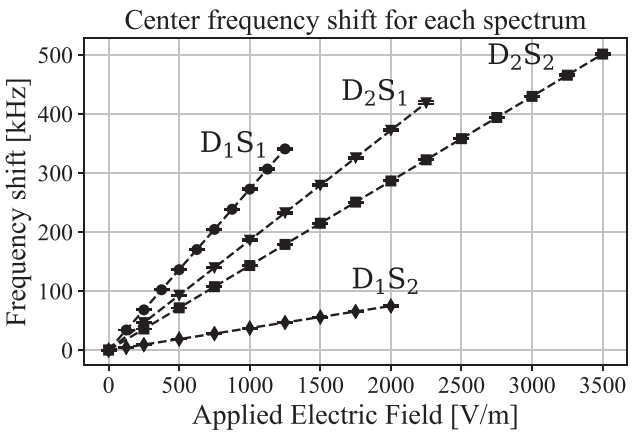

FIG. 4. The displacements of the center frequency of the spectral hole as a function of the amplitude of the E-field applied parallel to D_1 and D_2, for the two different crystal sites (S_1 and S_2), as well as linear fits to the data.

The uncertainty on the electric field is composed of three elements: applied voltage, crystal dimensions, and inhomogeneity of the electric field arising from an electrode geometrical misalignment and difference in permittivity between vacuum and YSO. The voltage and the crystal dimensions were verified using SI-traceable calibrated instruments, resulting in an error induced by these quantities significantly below the stated uncertainty. We performed numerical simulations using finite element method software, utilizing the permittivity coefficient of YSO expressed in Ref. 29 and allowing for up to 1 mm misalignment of the electrodes. These simulations confirm that, averaged over the part of the crystal probed by the laser beam, the relative error on the estimation of the electric field is below 3×10^{-6}, implying a negligible effect on our stated uncertainty. The statistical uncertainty on the coefficients is obtained from the linear fit, which takes into account the error bars on each individual frequency measurement, arising from the Lorentzian fits of each spectral pattern. The last column in Table I shows the systematic errors that arise from the

TABLE I. Linear Stark coefficients for europium ions in an YSO matrix when the electric field is applied parallel to one of the crystalline axes D_1 or D_2 and for crystal site 1 or 2. These coefficients are given in Hz per (V/m). $\pm$ and $\mp$ in the last column indicate that the D_1 and D_2 systematic errors go in opposite directions.

Site	Axis	Value	Stat.	Syst.
1	D_1	271.8	± 0.5	± 1.6
1	D_2	186.1	± 0.4	∓ 2.4
2	D_1	37.4	± 0.5	± 1.2
2	D_2	143.2	± 0.5	∓ 0.3

11 August 2023 11:59:53

Published under license by AIP Publishing

uncertainty on the orientation of the dielectric axis relative to the crystal-cut ($\pm 0.5°$, as set by x-ray orientation and precision machining). Note that during all measurements, we systematically probe the spectral structure without the E-field before and after the measurement sequence, to verify that no drift has occurred due to other independent physical variables during the measurement sequence.

For applications in which the narrow spectral feature is used for high precision laser frequency stabilization, the linear shifts due to small fluctuations of an electric field only broaden the peak symmetrically (an initial symmetric splitting) and, thus, do not change the frequency of a laser locked to this peak (only the slope of the frequency discriminator is changed, not its central position). What can potentially be more detrimental in such applications is a higher order Stark effects, which would introduce a non-symmetric behavior between the positive and negative branches and, thus, would result, for small electric field fluctuations, in laser frequency fluctuations. Due to the high precision in our frequency measurements, we can search for a quadratic component at relatively weak fields, despite the non-zero linear sensitivity, and set an upper limit of this type of non-linear Stark shift. We note that this kind of quadratic behavior physically corresponds to a small electric polarizability effect, where E-field-induced additional dipole moments in the ground and excited states, proportional to and along the E-field, produce a correction to the permanent $\delta\vec{\mu}_i$, in a direction (set by the E-field) that is identical for the classes of ions having opposite permanent dipole moments.

Contrary to the linear (symmetric) case, it is desirable here to explicitly correct for possible slow frequency drifts of the reference cavity, typically of the order of 0.1 Hz s^{-1}, resulting in an apparent drift of frequency of the initial spectral hole, i.e., $f_0 = 0$ no longer holds throughout the experimental sequence (which lasts longer than the stability specification timescale of the cavity). This correction is done by using an optical frequency comb, referenced to the primary frequency standard, which is constantly monitoring the probe laser optical frequency. The results are shown, for both directions and sites, in Fig. 5 in which we have plotted $\delta f_2 = (f_+ + f_-)/2 - f_0$ as a function of the applied E-field. We notice the absence of any clear trend corresponding to an asymmetric shift of the peaks in the data. Fitting (least squares method) with a purely quadratic function, $\delta f_2 = A_2 E^2$, we obtain the coefficients A_2 for the quadratic Stark effect expressed in Table II. These quadratic coefficient can be considered compatible with zero given the measurement uncertainties, and, as conservative estimates, we set the upper limits stated in the last column of the table. For site 1, this is coherent with the significantly less stringent limit of $\pm$ 0.2 $Hz^2\ V^{-2}$ previously obtained.[25,31]

When the peaks from the positive and negative branches separate under the application of an E-field, a final possibility of the quadratic effect corresponds to a deviation from the linear behavior, which would be symmetric between the positive and negative branches. This would physically require the field-induced part of $\delta\vec{\mu}_i$ to be aligned with $\delta\vec{\mu}_i$ rather than with the external E-field, but still be proportional to the amplitude of the field. Although this situation is physically more

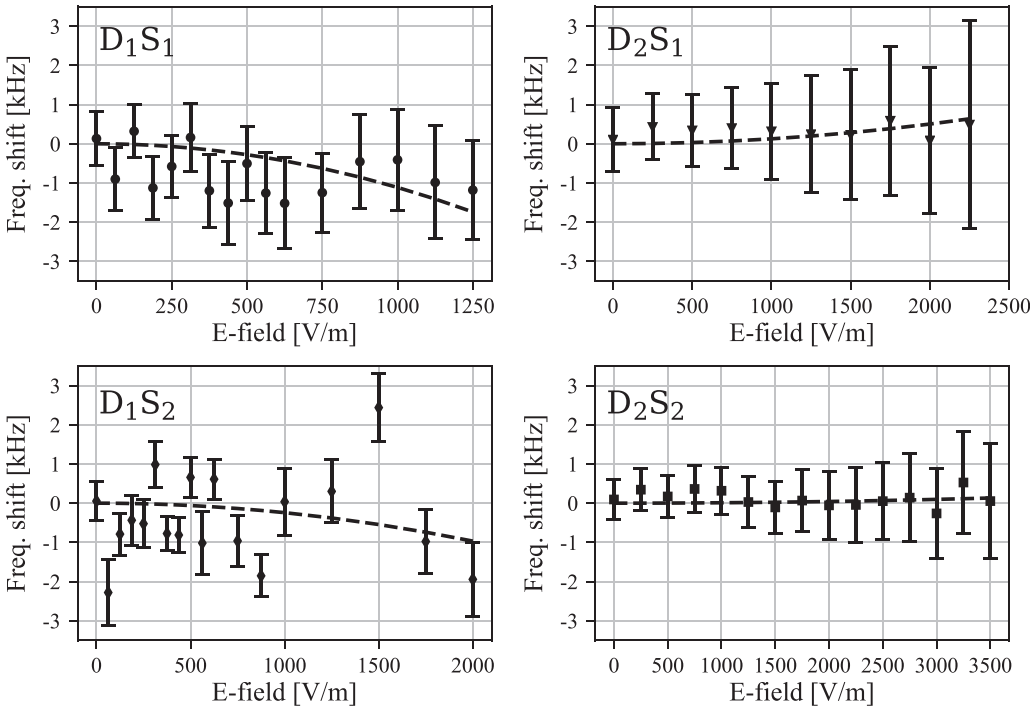

FIG. 5. Mean central frequency of the positive and negative branch peaks (with reference to the zero E-field case where the initial hole burning occurred) as a function of the applied E-field parallel to D_1 or D_2 and for site 1 (S_1) or site 2 (S_2), as indicated by the labels in the insets. The data have been corrected from the drift of the probe laser, which is continuously measured using a primary frequency referenced optical frequency comb. The dashed lines are a quadratic fit to these data, showing an effect compatible with zero to within the measurement uncertainty.

11 August 2023 11:59:53

Published under license by AIP Publishing

TABLE II. Quadratic Stark coefficients for residues after subtracting the linear component. These coefficients are given in Hz per (V/m)^2. The systematic error is, here, negligible compared to the statistic error.

Site	Axis	Value	Stat.	Abs. val. upper limit
1	D_1	-11.1×10^{-4}	$\pm 5.0 \times 10^{-4}$	$<3 \times 10^{-3}$
1	D_2	1.3×10^{-4}	$\pm 2.6 \times 10^{-4}$	$<1 \times 10^{-3}$
2	D_1	-2.4×10^{-4}	$\pm 1.4 \times 10^{-4}$	$<1 \times 10^{-3}$
2	D_2	0.1×10^{-4}	$\pm 0.5 \times 10^{-4}$	$<2 \times 10^{-4}$

difficult to interpret than the asymmetric quadratic Stark effect discussed above, we still investigate the data for the presence of such behavior. For simplicity, we only consider the positive branch and examine the residue after subtracting the linear Stark shift determined previously, i.e., $\delta f_{2,+} = f_+ - f_0 - A_1 E$. These residues are then fitted with a purely quadratic function, $\delta f_{2,+} = A_{2,+} E^2$. From the fitting procedure, we obtain quadratic coefficients for the D_1-direction of $(-1.3 \pm 5.1) \times 10^{-4}$ Hz^2 V^{-2} for site 1 and $(-0.7 \pm 1.5) \times 10^{-4}$ Hz^2 V^{-2} for site 2 and for the D_2-direction $(-0.5 \pm 2.6) \times 10^{-4}$ Hz^2 V^{-2} for site 1 and $(-0.1 \pm 0.5) \times 10^{-4}$ Hz^2 V^{-2} for site 2 (with negligible systematic uncertainties). Again, these coefficients are compatible with zero within the measurement uncertainty and they are all below $\pm$ 1 mHz^2 V^{-2}.

The spectral holes prior to applying an E-field typically exhibit an FWHM of approximately 3–5 kHz. When the E-field is increased, the spectral structures gradually broaden, as observed in Fig. 3. A minor part (approximately 10% by the end of five consecutive measurements) of this broadening is due to the probing beam, which slowly pumps ions from the edges of the spectral hole into dark states. In principle, the remaining part could be due to a spatial inhomogeneity in the applied field. Finite-element simulations show, however, that such an effect is very small (<1% of the linewidth), an assertion corroborated by experimental findings that 1) using a 6 mm diameter probe beam instead of 2 mm does not change the broadening and 2) highly E-field sensitive cases (e.g., D_1S_1) exhibit similar broadening as less sensitive ones (e.g., D_1S_2). However, a slight misalignment of the field (within the stated precision of crystal cutting) producing a component along the *b*-axis may explain most of the broadening (the positive and negative branches broaden symmetrically under such an effect). Going to higher E-fields, we have indeed observed a secondary splitting, which, extrapolated, accounts for at least 50% of the residual broadening. However, no matter the reason behind the broadening, the corresponding uncertainty is largely included in our error bars on the data and, thus, in the uncertainty stated for the Stark coefficients.

In this Letter, by means of direct probing of ultranarrow spectral structures, we have provided measurements of the linear Stark effect for an optical transition in Eu^{3+} ions in an Y_2SiO_5 matrix by applying a field parallel to the D_1 or D_2 axis, with an accuracy below the 3 Hz m V^{-1} level. Surprisingly, for an E-field applied parallel to the D_1-direction, crystal site 1 is a factor of seven more sensitive to the field than site 2. This is useful information for applications using E-fields to electrically tune the transition frequency. Moreover, our measurements have allowed us to provide an upper limit for both an asymmetric and symmetric quadratic Stark coefficient of the order of or below the 1 mHz^2 V^{-2} level, depending on the site, direction, and effect considered, important information for applications in which the electric field is a source of noise, such as metrology applications, in which the transition is used as a frequency reference. For example, in order to reach a relative frequency stability of 10^{-17} using a spectral hole as a frequency reference, an asymmetric quadratic Stark effect <1 mHz^2 V^{-2} translates into a requirement of the E-field instability below 2.3 V m^{-1}.

This project was supported by the European Union's Horizon 2020 research and innovation program under Grant Agreement No 712721 (NanOQTech). It also received support from the Ville de Paris Emergence Program, the Région Ile de France DIM SIRTEQ, the LABEX Cluster of Excellence FIRST-TF (No. ANR-10-LABX-48-01) within the Program "Investissements d'Avenir" operated by the French National Research Agency (ANR), and the EMPIR 15SIB03 OC18 program co-financed by the Participating States and the European Union's Horizon 2020 research and innovation program.

DATA AVAILABILITY

The data that support the findings of this study are available from the corresponding author upon reasonable request.

REFERENCES

[1] R. Yano, M. Mitsunaga, and N. Uesugi, "Ultralong optical dephasing time in Eu^{3+}: Y_2SiO_5," Opt. Lett. **16**, 1884 (1991).
[2] R. W. Equall, Y. Sun, R. L. Cone, and R. M. Macfarlane, "Ultraslow optical dephasing in Eu^{3+}: Y_2SiO_5," Phys. Rev. Lett. **72**, 2179 (1994).
[3] C. W. Thiel, T. Böttger, and R. L. Cone, "Rare-earth-doped materials for applications in quantum information storage and signal processing," J. Lumin. **131**, 353 (2011).
[4] P. Goldner, A. Ferrier, and O. Guillot-Noël, "Rare earth-doped crystals for quantum information processing," in *Handbook on the Physics and Chemistry of Rare Earths*, edited by J.-C. G. Bünzli and V. K. Pecharsky (Elsevier, 2015), Vol. 46, pp. 1–78.
[5] M. Rančić, M. P. Hedges, R. L. Ahlefeldt, and M. J. Sellars, "Coherence time of over a second in a telecom-compatible quantum memory storage material," Nat. Phys. **14**, 50 (2018).
[6] P. Berger, Y. Attal, M. Schwarz, S. Molin, A. Louchet-Chauvet, T. Chanelière, J.-L. L. Gouët, D. Dolfi, and L. Morvan, "RF spectrum analyzer for pulsed signals: ultra-wide instantaneous bandwidth, high sensitivity, and high time-resolution," J. Lightwave Technol. **34**(20), 4658 (2016).
[7] C. Venet, M. Bocoum, J.-B. Laudereau, T. Chanelière, F. Ramaz, and A. Louchet-Chauvet, "Ultrasound-modulated optical tomography in scattering media: Flux filtering based on persistent spectral hole burning in the optical diagnosis window," Opt. Lett. **43**, 3993 (2018).
[8] M. Nilsson and S. Kröll, "Solid state quantum memory using complete absorption and re-emission of photons by tailored and externally controlled inhomogeneous absorption profiles," Opt. Commun. **247**, 393 (2005).
[9] F. Bussières, C. Clausen, A. Tiranov, B. Korzh, V. B. Verma, S. W. Nam, F. Marsili, A. Ferrier, P. Goldner, H. Herrmann, C. Silberhorn, W. Sohler, M. Afzelius, and N. Gisin, "Quantum teleportation from a telecom-wavelength photon to a solid-state quantum memory," Nat. Photonics **8**, 775–778 (2014).
[10] A. Walther, L. Rippe, Y. Yan, J. Karlsson, D. Serrano, A. N. Nilsson, S. Bengtsson, and S. Kröll, "High-fidelity readout scheme for rare-earth solid-state quantum computing," Phys. Rev. A **92**, 022319 (2015).
[11] N. Maring, P. Farrera, K. Kutluer, M. Mazzera, G. Heinze, and H. de Riedmatten, "Photonic quantum state transfer between a cold atomic gas and a crystal," Nature **551**, 485 (2017).
[12] A. M. Dibos, M. Raha, C. M. Phenicie, and J. D. Thompson, "Atomic source of single photons in the telecom band," Phys. Rev. Lett. **120**, 243601 (2018).
[13] T. Zhong, J. M. Kindem, J. G. Bartholomew, J. Rochman, I. Craiciu, E. Miyazono, M. Bettinelli, E. Cavalli, V. Verma, S. W. Nam, F. Marsili, M. D. Shaw, A. D. Beyer, and A. Faraon, "Nanophotonic rare-earth quantum memory with optically controlled retrieval," Science **357**(6358), 1392 (2017).

11 August 2023 11:59:53

Published under license by AIP Publishing

[14]C. Laplane, P. Jobez, J. Etesse, N. Gisin, and M. Afzelius, "Multimode and long-lived quantum correlations between photons and spins in a crystal," Phys. Rev. Lett. **118**, 210501 (2017).
[15]A. Seri, A. Lenhard, D. Rieländer, M. Gündoğan, P. M. Ledingham, M. Mazzera, and H. de Riedmatten, "Quantum correlations between single telecom photons and a multimode on-demand solid-state quantum memory," Phys. Rev. X **7**, 021028 (2017).
[16]B. Julsgaard, A. Walther, S. Kröll, and L. Rippe, "Understanding laser stabilization using spectral hole burning," Opt. Express **15**, 11444 (2007).
[17]M. J. Thorpe, L. Rippe, T. M. Fortier, M. S. Kirchner, and T. Rosenband, "Frequency stabilization to 6×10^{-16} via spectral-hole burning," Nat. Photonics **5**, 688 (2011).
[18]N. Galland, N. Lučić, S. Zhang, H. Alvarez-Martinez, R. Le Targat, A. Ferrier, P. Goldner, B. Fang, S. Seidelin, and Y. Le Coq, "Double-heterodyne probing for ultra-stable laser based spectral hole burning in a rare-earth doped crystals," Opt. Lett. **45**, 1930 (2020).
[19]N. Galland, N. Lučić, B. Fang, S. Zhang, R. Le Targat, A. Ferrier, P. Goldner, S. Seidelin, and Y. Le Coq, "Mechanical tunability of an ultranarrow spectral feature via uniaxial stress," Phys. Rev. Appl. **13**, 044022 (2020).
[20]S. Zhang, N. Galland, N. Lučić, R. Le Targat, A. Ferrier, P. Goldner, B. Fang, Y. Le Coq, and S. Seidelin, "Inhomogeneous response of an ion ensemble from mechanical stress," Phys. Rev. Res. **2**, 013306 (2020).
[21]K. Mølmer, Y. Le Coq, and S. Seidelin, "Dispersive coupling between light and a rare-earth-ion-doped mechanical resonator," Phys. Rev. A **94**, 053804 (2016).
[22]S. Seidelin, Y. Le Coq, and K. Mølmer, "Rapid cooling of a strain-coupled oscillator by an optical phase-shift measurement," Phys. Rev. A **100**, 013828 (2019).
[23]R. M. Macfarlane, "Optical Stark spectroscopy of solids," J. Lumin. **125**, 156 (2007).
[24]Q. Li, Y. Bao, A. Thuresson, A. N. Nilsson, L. Rippe, and S. Kröll, "Slow-light-based optical frequency shifter," Phys. Rev. A **93**, 043832 (2016).
[25]F. R. Graf, "Investigations of spectral dynamics in rare earth ion doped crystals using high resolution laser techniques," Ph.D. thesis (ETH Zürich, 1998).
[26]R. M. Macfarlane, A. Arcangeli, A. Ferrier, and P. Goldner, "Optical measurement of the effect of electric fields on the nuclear spin coherence of rare-earth ions in solids," Phys. Rev. Lett. **113**, 157603 (2014).
[27]F. Könz, Y. Sun, C. W. Thiel, R. L. Cone, R. W. Equall, R. L. Hutcheson, and R. M. Macfarlane, "Temperature and concentration dependence of optical dephasing, spectral-hole lifetime, and anisotropic absorption in Eu^{3+}: Y_2SiO_5," Phys. Rev. B **68**, 085109 (2003).
[28]O. Gobron, K. Jung, N. Galland, K. Predehl, R. Letargat, A. Ferrier, P. Goldner, S. Seidelin, and Y. Le Coq, "Dispersive heterodyne probing method for laser frequency stabilization based on spectral hole burning in rare-earth doped crystals," Opt. Express **25**, 15539 (2017).
[29]N. C. Carvalho, J.-M. Le Floch, J. Krupka, and M. Tobar, "Multi-mode technique for the determination of the biaxial Y_2Si0_5 permittivity tenssor from 300 to 6K," Appl. Phys. Lett. **106**, 192904 (2015).
[30]F. R. Graf, A. Renn, U. P. Wild, and M. Mitsunaga, "Site interference in Stark-modulated photon echoes," Phys. Rev. B **55**, 11225 (1997).
[31]M. J. Thorpe, D. R. Leibrandt, and T. Rosenband, "Shifts of optical frequency references based on spectral-hole burning in Eu^{3+}: Y_2SiO_5," New J. Phys. **15**, 033006 (2013).

11 August 2023 11:59:53

Published under license by AIP Publishing